Title

Modeling seeding and neuroanatomic spread of pathology in amyotrophic lateral sclerosis

Authors

Pandya, Sneha

Maia, Pedro D

Freeze, Benjamin

et al.

Publication Date

2022-05-01

DOI

10.1016/j.neuroimage.2022.118968

Peer reviewed

Published in final edited form as:

Neuroimage. 2022 May 01; 251: 118968. doi:10.1016/j.neuroimage.2022.118968.

Modeling seeding and neuroanatomic spread of pathology in amyotrophic lateral sclerosis

Sneha Pandya[a], **Pedro D. Maia**[b], **Benjamin Freeze**[c], **Ricarda A. L. Menke**[d], **Kevin Talbot**[e], **Martin R. Turner**[d,e,*], **Ashish Raj**[a,f,**]

[a]Department of Radiology, Weill Cornell Medicine, 1300 York Avenue, New York, NY, United States

[b]Department of Mathematics, University of Texas at Arlington, TX, United States

[c]Scripps Health/MD Anderson Cancer Center, Department of Radiology, CA, United States

[d]Wellcome Centre for Integrative Neuroimaging, University of Oxford, West Wing Level 6, Oxford OX2 7PZ, United Kingdom

[e]Nuffield Department of Clinical Neurosciences, University of Oxford, Oxford, United Kingdom

[f]Department of Radiology and Biomedical Imaging, University of California, San Francisco, CA 94121, United States

Abstract

The neurodegenerative disorder amyotrophic lateral sclerosis (ALS) is characterized by the progressive loss of upper and lower motor neurons, with pathological involvement of cerebral motor and extra-motor areas in a clinicopathological spectrum with frontotemporal dementia (FTD). A key unresolved issue is how the non-random distribution of pathology in ALS reflects differential network vulnerability, including molecular factors such as regional gene expression, or preferential spread of pathology via anatomical connections. A system of histopathological staging of ALS based on the regional burden of TDP-43 pathology observed in *postmortem* brains has been supported to some extent by analysis of distribution of in vivo structural MRI changes. In this paper, computational modeling using a Network Diffusion Model (NDM) was used to investigate whether a process of focal pathological 'seeding' followed by structural network-based spread recapitulated *postmortem* histopathological staging and, secondly, whether this had any correlation

[**]Address correspondence to: Ashish Raj, Professor of Radiology and Bio-Engineering, 185 Berry Street, Suite 370, University of California at San Francisco, San Francisco, CA 94121. Ashish.Raj@ucsf.edu (A. Raj). [*]Address correspondence to: Prof Martin Turner, West Wing Level 6, John Radcliffe Hospital, Oxford OX2 7PZ, UK. martin.turner@ndcn.ox.ac.uk (M.R. Turner).

Author contributions

Sneha Pandya: Conceptualization, Methodology, Software, Writing-Original draft preparation, Visualization, Investigation, Writing-Reviewing and Editing. **Pedro Maia:** Software, Writing-Reviewing and Editing. **Ben Freeze:** Software, Writing-Reviewing and Editing. **Ricarda Menke:** Resources, Validation. **Kevin Talbot:** Resources, Validation. **Martin Turner:** Supervision, Writing-Original draft preparation, Validation. **Ashish Raj:** Supervision, Conceptualization, Methodology, Writing-Original draft preparation, Validation, Writing-Reviewing and Editing.

Declaration of Competing Interest

Authors report no competing interest.

Supplementary materials

Supplementary material associated with this article can be found, in the online version, at doi: 10.1016/j.neuroimage.2022.118968.

to the pattern of expression of a panel of genes implicated in ALS across the healthy brain. Regionally parcellated T1-weighted MRI data from ALS patients (baseline n = 79) was studied in relation to a healthy control structural connectome and a database of associated regional cerebral gene expression. The NDM provided strong support for a structural network-based basis for regional pathological spread in ALS, but no simple relationship to the spatial distribution of ALS-related genes in the healthy brain. Interestingly, OPTN gene was identified as a significant but a weaker non-NDM contributor within the network-gene interaction model (LASSO). Intriguingly, the critical seed regions for spread within the model were not within the primary motor cortex but basal ganglia, thalamus and insula, where NDM recapitulated aspects of the *postmortem* histopathological staging system. Within the ALS-FTD clinicopathological spectrum, non-primary motor structures may be among the earliest sites of cerebral pathology.

1. Introduction

Amyotrophic lateral sclerosis (ALS), the commonest phenotype of motor neuron disease, is a progressive and fatal neurodegenerative disorder with complex molecular underpinnings (Talbot et al., 2018). The disease is clinically characterized by the progressive loss of upper motor neurons in the primary motor cortex and corticospinal tract and lower motor neurons of the spinal cord and brainstem. However ALS also involves extra-motor cerebral systems, with clear pathological, genetic and clinical overlap with frontotemporal dementia (FTD) (Es et al., 2017), with the behavioral variant being most common. Advances in neuroimaging have revealed many aspects of pathogenesis across the ALS-FTD spectrum (Turner et al., 2013; Chiò et al., 2014), with increasing interest in its potential to deliver therapeutic outcome measures (Menke et al., 2017).

The pattern of clinical symptom spread in ALS (Ravits et al., 2007b; Turner et al., 2010) and the associated spinal cord pathology (Ravits and La Spada, 2009), is not random but is focal in onset and spreads contiguously. Nearly all cases of ALS and around 50% of FTD are associated with cytoplasmic neuronal and glial inclusions of aggregated 43 kDa transactive response DNA-binding protein, TDP-43 (Neumann et al., 2006). *Postmortem* histopathological classification has been interpreted as evidence of a stereotyped pattern of cerebral pathological involvement in ALS (Brettschneider et al., 2013). Several molecular mechanisms have been proposed to explain the apparent selective vulnerability of motor neurons. These include cell-autonomous factors, involving oxidative stress, excitotoxicity, and mitochondrial dysfunction (Turner et al., 2013) and non cell-autonomous factors involving cell-cell communication (e.g. glia (Philips and Rothstein, 2014)) or trans-neuronal transmission of aggregate-prone proteins through prion-like templating (Polymenidou and Cleveland, 2011; Riku, 2020), in which network connectivity might define the canonical pattern of spread (Seeley et al., 2009).

It is not yet clear how molecular vulnerability and network connectivity might combine in mediating regional patterns of pathology in ALS. Like other neurodegenerative diseases, the spatial topography of ALS histopathology is not related in a simple way to regional expression of genes implicated in pathogenesis (Fusco et al., 1999; Jackson, 2014; Subramaniam, 2019). A high level of clinical and molecular heterogeneity in the ALS-FTD

syndrome meanwhile hamper the ability to map its course in a precise manner to facilitate effective therapeutic trials (Turner and Swash, 2015).

In this paper we address these issues using computational modeling, gene expression analysis and large observational imaging studies in ALS, combined with prior histopathological staging data. We interrogate whether focal seeding followed by structural network-based spread recapitulate patterns of ALS pathology by employing a Network Diffusion Model (NDM) to map neurodegenerative topography (Raj et al., 2012). This model was successful in recapitulating spatial patterns of diverse proteinopathies including Alzheimer's (Raj et al., 2015), frontotemporal dementia (Raj et al., 2012), Parkinson's disease (Freeze et al., 2018, 2019; Pandya et al., 2019), Huntington's disease (Poudel et al., 2019), Traumatic brain injury (Poudel et al., 2020) and progressive supranuclear palsy (Pandya et al., 2017). We also include spatial transcriptomic analysis in this framework, to understand the role of innate regional vulnerability in ALS.

2. Methods

2.1. Participants

Data used in this study were obtained after informed consent from participants in the longitudinal Oxford Study for Biomarkers in Motor Neuron Disease ('BioMOx') cohort based on referrals to a large tertiary ALS clinic and clinical assessment involving two experienced neurologists (KT, MRT). For the purposes of this group-level analysis, a diagnosis of ALS included those within all El Escorial clinical diagnostic categories at baseline (including those with pure upper or lower motor neuron syndromes clinically) who also showed clear progression of motor involvement in subsequent follow-up. Data were available for 79 such ALS participants (mean age at baseline 61 ± 11 years, male:female 2:1, mean duration from symptom onset 49 ± 57 months). Of these, 48 were also able to undergo repeat MRI every 6 months to a maximum of 5 visits in total (cohort overlaps with (Menke et al., 2018)). One baseline participant initially labelled as ALS was removed from the study cohort later due to failure to progress. MRI and cognitive data were obtained for thirty-nine age matched normal during a single visit (cohort overlaps with (Proudfoot et al., 2015)). All ALS participants were apparently sporadic (i.e. no family history of ALS or FTD). The study predated routine genetic testing in the clinic, but subsequent experience predicts this would have identified up to 3 apparently sporadic ALS gene mutation carriers, which is not felt to be material to the outcome. Demographic and clinical details of the participants are shown in Table SI – 1.

2.2. Image acquisition and regional volumetric analysis

Images were acquired using a 3T Siemens Trio scanner (Siemens AG) with a 12-channel head coil at the Oxford center for Clinical Magnetic Resonance (OCMR). A high resolution 3D MP-RAGE T1-weighted sequence was obtained for each subject with the following parameters: 192 axial slices; repetition and echo time (TR/TE) = 2040/4.7 ms, flip angle 8°, $1 \times 1 \times 1$ mm^3 voxel size, and 6 min acquisition time.

MRI images were mapped to Freesurfer's Desikan-Killany atlas. 68 cortical and 18 subcortical volumes from these MRI images were extracted using FreeSurfer software with a cross-sectional pipeline for both the cohorts. Regional volumes were normalized by total intracranial volume generated by FreeSurfer to correct for head size. Image processing steps were visually inspected for white–gray matter boundary and skull-stripping errors to ensure they had been carried out correctly. 6 subjects that rated either 'partial' or 'fail' due to FreeSurfer failure or insufficient tissue contrast were excluded from analysis. A vector of regional atrophy was created by using a two tailed t-test between ALS and normal mean ICV corrected regional volumes such that $t_{\mathrm{ALS}} = \{t_{\mathrm{ALS}}(i) \mid i \in [1, N]\}$ ($N = 86$). The t-statistic was converted to the natural positive range between 0 and 1 using the logistic transform given by $\Phi = 1/(1 + \exp(-(t_{ALS} - \mathrm{a0})//\sigma/std(t_{ALS}))$, where, $\sigma = 2$ and $\mathrm{a0} = 0.5^{*}\ \sigma$ (Raj et al., 2015). This transformation maps t-values such that they asymptotically approach 0 as t_{ALS} approaches $-\infty$ and 1 as t_{ALS} approaches $+\infty$. The parameter σ controls the steepness of the logistic function. These atrophy measures were then used to test the propagation modeling analyses using NDM.

2.3. A healthy structural connectome

Axial T1-weighted structural MRI scans using fast spoiled gradientecho sequence(TE = 1.5 ms, TR = 6.3 ms, TI = 400 ms, 15° flip angle, 230 × 230 × 156 isotropic 1 mm voxels) and high angular resolution diffusion tensor imaging data (DTI) (55 directions, b = 1000 s/mm2, 72 1.8-mm-thick interleaved slices, 0.8594 mm × 0.8594 mm planar resolution) were acquired on a 3T GE Signa EXCITE scanner from fully consented 73 young healthy volunteers under a previous study approved by Weill Cornell's institutional review board (Kuceyeski et al., 2013). Thus, the cohort used to extract a healthy structural connectome was different from the 39 age-matched controls described earlier, that was used for determining regional atrophy. Probabilistic tractography was performed on the diffusion MRI data after seeding each voxel at the interface of the WM and GM boundary. The resulting streamlines were binned into subsets corresponding to every pair of GM regions given by the parcellation scheme described above. The anatomical connection strength (ACS), a measure of connectivity, was used in this paper (Iturria-Medina et al., 2007). ACS is defined as the weighted sum of the streamlines found to exist between any pair of gray matter structures, weighted by each streamline's probability score. The ACS is further normalized by a scaling factor equaling to the total sum of all streamlines. We define $c_{i,j}$, as the resulting connection strength between i^{th} and j^{th} GM regions. We refer to the matrix collecting all pair-wise entries as the connectivity matrix $C = \{c_{i,j}\}$. Here the ACS is used as an approximation of the cross-sectional area of all axonal projections connecting two regions – a plausible choice given our goal of modeling the amount of pathology transmission conducted through these projections. Connections are assumed to be bidirectional since directionality is not deducible from DTI tractography data.

2.4. NDM for ALS pathology spread

The hypothetical spread of disease-causing proteinopathy into the network represented by the connectivity matrix C over time t can be captured by starting a diffusion process from a "seed " region. Since we do not know *a priori* which region is the likely seed, we select

every brain region as the seed region, one at a time (Raj et al., 2012). The overall strategy is to simulate a diffusion process on the connectivity graph for many time points, starting from each seed location, while recording its correlation with measured regional atrophy maps.

We modeled ALS progression as a diffusion process of the pathology load x on the graph C over model time t. From (Raj et al., 2012) the transmission of pathology from region 1 to region 2 is represented as $\frac{dx_1}{dt} = \beta c_{1,2}(x_2 - x_1)$ where x_1 and x_2 denote the magnitude of disease-causing pathology in each region, and β is a global diffusivity constant. Denoting pathology from all regions i into a vector $\mathbf{x}(t) = \{x_i(t)\}$, the above equation extends to become:

$$\frac{d\mathbf{x}(t)}{dt} = -\beta H\mathbf{x}(t) \quad (1)$$

where H is the well-known graph Laplacian

$$H = I - D^{-\frac{1}{2}}CD^{-\frac{1}{2}} \quad (2)$$

where D is a diagonal matrix whose diagonal entries contain the degree of each node, degree being defined as the sum of weighted connections emanating from the node. Note, in order to accommodate regions having widely different out-degrees, we used the degree-normalized version of the Laplacian matrix (Raj et al., 2015). Eq. 1 admits a closed-form solution $\mathbf{x}(t) = e^{-\beta Ht}\mathbf{x}_0$ where $\mathbf{x}_0$ is the initial pattern of the disease process at $t = 0$, and we call term $e^{-\beta Ht}$ the *diffusion kernel* since it acts essentially as a spatial and temporal blurring operator on $\mathbf{x}_0$. The unit of the model's diffusion time t is arbitrary (au). The exact value of global diffusivity β is unknown, hence we chose a value that would roughly span ALS disease progression (3–10 years). Specifically, we chose a β such that the peak correlation of the NDM against empirical atrophy will occur, over all seeded regions, in the range $t_{max} \in [3, 10]$ *years*. We ran NDM for multiple β values that would satisfy above criteria. In our experimentation, we achieved this for $\beta = 1$.

The NDM is described by pathology $x(t)$ and our hypothesis is that it should correlate with empirical atrophy Φ. Pearson correlation strength (R statistic) and p-values were calculated between the (static) empirical atrophy measured on the ALS group Φ and x(t) at all model timepoints t.

Repeated seeding—The NDM was run for all 86 seed regions, each time starting from a different ROI, such that $\mathbf{x}_0$ is a unit vector with 1 at the index of the seed and zeros at all other regions. We observed that the atrophy pattern in our group was generally bilateral, hence for repeated seeding experiments, we chose to seed bilaterally, so that two entries in the "unit " vector were assigned 1. This was repeated for each region in turn, and the NDM-predicted pathology pattern was calculated. The Pearson's correlation coefficient R was computed between each predicted pathology vector $x^i(t)$ seeded at region i and the empirical pathology vector Φ over all model timepoints t, giving $R^i(t)$. "R-t curves" were represented

by plotting these $R^i(t)$ values on common axis. R^i_{max} was recorded as the maximum value from each $R^i(t)$, which reflected the likelihood of i-th region as the true region of pathology onset. In this study we included seed regions in computing R_{max}. In addition, we re-ran NDM with ACS connectome and excluded seed regions in computing R_{max}, and also with connectome derived from human connectome project (HCP) and Euclidean distance for further validation.

Histopathological staging.—We tested whether NDM recapitulated the *postmortem* histopathological staging published in ALS (Brettschneider et al., 2013), assigning each of the 86 regions available in our atlas an ALS stage from 1 to 4. Regions that were not part of this staging schema were arbitrarily assigned stage 5, a category that denotes the least vulnerable regions X. In our study we largely followed the staging scheme from (Brettschneider et al., 2013) rather than (Schmidt et al., 2016), but with a few changes in order to achieve a more graded mapping of TDP-43 implicated regions. Since we wanted to map all 86 regions of the Desikan-Killany atlas, we used (Brettschneider et al., 2013) to assign stages to most prefrontal and temporal areas, while (Schmidt et al., 2016) did a much less granular mapping (Table 1 in (Schmidt et al., 2016)). Those regions that were differently mapped between our study and (Schmidt et al., 2016) are mainly in frontal and temporal areas, and reflect our understanding from Brettschneider and additional inputs from the wider literature (Braak et al., 2013, 2017; Cykowski et al., 2014; Braak and Del Tredici, 2018; Kawakami et al., 2019).

Spatiotemporal evolution from most likely seed regions.—The top five regions i with the highest R_{max} were chosen to qualify as best seeds, along with the precentral gyrus which is considered a key early site of ALS. We tabulated a similar list of top 5 seed regions that gave the highest Pearson correlation (R_{TDP43}) between the NDM and the ALS TDP-43 pathology staging data. An average of these two Pearson correlation values (R_{avg}) was computed from both empirical atrophy and TDP-43 staging after taking an absolute of R_{TDP43} values. The regions with the highest R_{avg} were considered as the best seeds overall and were used as seeding locations for further analysis (see Results).

Regional gene expression analysis.—Prominent genes linked to familial ALS were (n = 25) identified from various studies (Robberecht and Eykens, 2015; Smith et al., 2017; Vajda et al., 2017; Chia et al., 2018; Karch et al., 2018; Nicolas et al., 2018) and mapped to 86 regions in the Desikan-Killiany atlas as in (Freeze et al., 2018). Additionally, genes in which pathogenic variants have been associated with TDP-43 pathology (n = 26) (Scotter et al., 2015) were also mapped to 86 regions as above. A list of all the genes used in this study can be found in the supplementary data. For each gene, data were obtained from six-post mortem brains provided by the human Allen Brain Atlas (AHBA) (Hawrylycz et al., 2012). Since only two of the six brains included samples from the right hemisphere, analyses were conducted from microarray gene expressions obtained from these two donors that had full spatial coverage. We used **abagen** toolbox (Markello et al., 2021) to reliably and robustly process and map gene expressions to the 86 regions of the Desikan-Killiany atlas.

Briefly, the regional microarray expression data were obtained from 2 postmortem brains provided by the AHBA. Data were processed with the abagen toolbox (version 0.1.3) using a 86-region volumetric atlas in MNI space. First, microarray probes were reannotated using data provided by (Arnatkeviciute et al., 2019) instead of the default probe information available with the AHBA; probes not matched to a valid Entrez ID were discarded. Next, probes were filtered based on their expression intensity relative to background noise, such that probes with intensity less than the background in >=50.00% of samples across donors were discarded, yielding 30,534 probes. When multiple probes indexed the expression of the same gene, we selected and used the probe with the most consistent pattern of regional variation across donors (i.e., differential stability). The MNI coordinates of tissue samples were updated to those generated via non-linear registration using the Advanced Normalization Tools. Samples were assigned to brain regions in the provided atlas if their MNI coordinates were within 2 mm of a given parcel. To reduce the potential for misassignment, sample-to-region matching was constrained by hemisphere and gross structural divisions (i.e., cortex, subcortex/brainstem, and cerebellum, such that e.g., a sample in the left cortex could only be assigned to an atlas parcel in the left cortex). If a brain region was not assigned a tissue sample based on the above procedure, every voxel in the region was mapped to the nearest tissue sample from the donor in order to generate a dense, interpolated expression map. The average of these expression values was taken across all voxels in the region, weighted by the distance between each voxel and the sample mapped to it, in order to obtain an estimate of the parcellated expression values for the missing region. Inter-subject variation was addressed by normalizing tissue sample expression values across genes using a robust sigmoid function. Normalized expression values were then rescaled to the unit interval. Gene expression values were then normalized across tissue samples using an identical procedure. All available tissue samples were used in the normalization process regardless of whether they were matched to a brain region; however, normalization was performed separately for samples in distinct structural classes (i.e., cortex, subcortex/brainstem, cerebellum). Tissue samples not matched to a brain region were discarded after normalization. Samples assigned to the same brain region were averaged separately for each donor and then across donors, yielding a regional expression matrix with 86 rows, corresponding to brain regions, and 15,329 columns, corresponding to the retained genes.

2.5. Statistical analyses

Throughout this paper the primary test statistic used to evaluate all models was Pearson's correlation strength R. In each case the dependent variable was the vector of regional atrophy or ALS staging, while the dependent variables were the NDM-predicted regional vector, and/or regional gene expression. As described above, R was computed at each model time t and the highest value was chosen as the model evidence.

For the gene results, genes for each category were corrected for multiple comparisons using Bonferroni method, with thresholded $p_{corr} = 0.05/25 = 0.002$ for ALS-related genes and thresholded $p_{corr} = 0.05/22 = 0.0023$ for TDP-43 specific genes. Correlation coefficients with p-values less than p_{corr} were considered statistically significant. Next, L_1 regularized regression model was created containing NDM from the seed region at $t_{max}(\mathbf{x}_{t\,max}^{seed})$ and regional

genetic expression profiles. Where, t_{max} is the time at which R_{max} is achieved between the predicted pathology and the empirical pathology for each region from the repeated seeding. Leave-one-out cross-validation was performed for each model by setting k to total number of samples across a range of values for the tuning parameter lambda (λ) using the Matlab script 'lasso'. These mapped genes and $\mathbf{x}_{t\,max}^{seed}$ were then linearly correlated with the atrophy using Matlab's 'fitlm' multiple linear regression script to achieve significant predictors for atrophy. Predictors for each lasso were corrected for multiple comparisons using Bonferroni method, with thresholded $p_{corr} = 0.05/(1 + 25 + 22) = 0.0010$ for $\mathbf{x}_{t\,max}^{seed}$, ALS-related genes, and TDP-43 specific genes. Correlation coefficients with p-values less than p_{corr} were considered statistically significant.

Random scrambling.—In order to build a null distribution for assigning significance to the NDM, we performed two levels of randomization experiments. 1) We ran the NDM on 2000 randomly scrambled versions of the connectivity matrix C. C was scrambled using a symmetric transformation of the network's nodes by randomly permuting entire rows and columns, and the NDM was evaluated for each shuffled network after bilateral Insula (In) seeding. This scrambling procedure maintains the edge and node statistics of the true connectivity C. The NDM evaluated on these 2000 randomly scrambled networks therefore constitute null or reference models which supplied significance values to results of the true model. 2) We ran the NDM on 2000 randomly scrambled ALS atrophy vector. Atrophy values in t_{norm} vector were randomly assigned amongst the 86 cerebral regions with 2000 different permutations. This scrambling method maintained the true connectivity C but replaced true regional atrophy pattern with a random distribution of atrophy.

2.6. Data availability

All data used in this study will be made available upon reasonable request and relevant code will be uploaded to https://github.com/Raj-Lab-UCSF repository. Oxford's Wellcome center for Integrative Neuroimaging has an inherent commitment to data-sharing. To get access to the data and comply with the research ethics committee approval an application to the corresponding author will be required so that the precise geographical extent of sharing is known.

3. Results

3.1. Spatial distribution of ALS atrophy and repeated seeding of the NDM

Fig. 1A shows glass-brain (LoCastro et al., 2014; Marinescu et al., 2019) illustrations of spatial distribution of ALS atrophy from our cross-sectional cohort which is consistent with progression of ALS pathology (Kassubek et al., 2005; Grosskreutz et al., 2006; Mezzapesa et al., 2007; Agosta et al., 2010; Westeneng et al., 2015). Severity of disease in each region is proportional to the t-statistic of ALS atrophy after logistic transform, where color towards red show increased severity. Table SI – 2 shows empirical atrophy values of top 20 regions averaged across both the hemispheres.

Each region was computationally seeded in succession and the NDM evolved over model time t on the healthy connectome C. The spatial distribution of R_{max}, which is indicative of

the likelihood of each region as a seed is depicted (Fig. 1B). Fig. 1C and Fig. 1D shows the distribution of empirical atrophy and R_{max} for each of these 86 regions alongside and a scatter plot respectively, which indicates that the NDM-derived seeding propensity value (R_{max}) does not simply reproduce the regions displaying the highest atrophy but instead reflects the consequence of network transmission starting from that region.

Fig. 1E shows the R-t curve revealing spread of R_{max} corresponding to the best fit between empirical data and the NDM seeded at the ith region (Eq. 2). For each region, the R-t curve would yield an intermediate peak in R, resembling the best match between the NDM and empirical data, and then after diffusing uniformly with decreasing resemblance between the actual data and the NDM. Table SI 3 shows top 20 regions with maximum Pearson correlation strength for each region seeded in succession. We show four sets of results: a) NDM is evaluated on our chosen ACS connectome, and the seed region is included in the calculation of Pearson correlation ($NDM_{ACS}^{Incl\ Seeds}$); b) NDM is evaluated on the ACS connectome, but seed region is excluded from correlation calculation ($NDM_{ACS}^{Excl\ Seeds}$); c) NDM is evaluated on an alternative HCP connectome (NDM_{HCP}); and d) NDM is evaluated on a distance graph whose edges are monotonically decreasing function of the Euclidean distance between region centroids ($NDM_{Euc\ Dist}$). Basal ganglia structures and the insula were among the top best seed regions for predicting ALS atrophy (Table SI – 3 - $NDM_{ACS}^{Incl\ Seeds}$), with the insula serving as the most likely seed region for ALS with the highest R_{avg} as seen in Table 1. Table SI – 3 - $NDM_{ACS}^{Excl\ Seeds}$ shows R_{max} resulting from seed exclusion which are either equal to or higher than the previous ones, suggesting that model's fitting is not overly influenced by the seed region's atrophy. Repeated seeding when replicated with HCP connectome resulted in similar Pearson correlation strength between different seed regions (Table SI – 3 - NDM_{HCP}). The R values are generally higher than with ACS, albeit with lower variability between seeding sites. The order of seeding sites is generally consonant with the ACS results, with thalamus (Th), insula and striatum being prominent in both. When the model is simulation on the Euclidean distance graph (Table SI – 3 - $NDM_{Euc\ Dist}$), the resulting R values are generally much lower than those from connectivity graphs (ACS or HCP). Thus, the evidence for proximity-based spread of ALS pathology is not as strong as evidence for spread on the connectivity graph.

To test whether the above results on group regional data and generic ALS staging data are also applicable to individual ALS subjects, we also ran NDM on ALS individuals and calculated maximum Pearson's R after seeding each of 43 bilateral ROIs for each subject. Peak R is achieved by frontal, parietal, temporal and subcortical regions, with frontal and subcortical regions achieving $R_{max} > 0.4$ from most subjects (Fig. 1F). Thus, there is considerable inter-subject heterogeneity in seeding, while at the group level there is a convergence of the likely seeds in frontoinsular and basal ganglia regions. In addition, we show distribution of seed likelihood in individual subjects when NDM is ran from a single seed Fig. 2A and when ran from everyone's best seeds Fig. 2B. We selected insula as a single seed given its obvious choice from our group level approach. Maximum R of 0.4642 was achieved when NDM was ran from insula seeding for individual subjects. Maximum Pearson's R obtained after seeding each of 43 bilateral ROI's for each subject were treated as best seeds. Maximum R of 0.5789 was obtained when NDM was ran from

best seeds from the individual subjects. We further correlated R_{max} obtained by the NDM fitting of individual subjects as described above, using both individual seeding and insula seeding with two ALS-specific clinical scores: UMN and ALSFRS clinical scores. These correlations are shown in Table 2.

3.2. Comparison with histopathological staging

Table 3 shows ALS staging for TDP-43 pathology in each region. As shown in Fig. 3 MRI atrophy and ALS staging are not highly correlated (R = −0.27), hence we wished to assess whether our model is also able to recapitulate *postmortem* histopathological staging. Therefore, the most likely seeding location for NDM was determined based on criteria that worked best for both atrophy and histopathological staging. Based on this criterion, the insula was selected as the best seed and used to play out NDM for all subsequent analyses (Table 1). Empirical atrophy, $\mathbf{x}^{In}_{i\,max}$, and staging maps are shown in Fig. 3A, 3B, and 3C respectively. Fig. 3B shows the distribution of predicted atrophy as determined by $\mathbf{x}^{In}_{i\,max}$. Pathology severity in each region is proportional to the color gradient. Regions with maximum severity as indicated by the NDM corresponded to regions in the more advanced histopathological stages, and is additionally statistically backed up by Fig. 3D,E. Given that seeding from the thalamus consistently produced the best R against empirical data (Fig. 1E, Table SI – 3), results were also obtained from $\mathbf{x}^{Th}_{i\,max}$ (Figure SI – 1). This demonstrated bilateral volume loss mainly occurring in regions corresponding to advanced histopathological staging.

3.3. Spatiotemporal evolution of ALS atrophy

The spatiotemporal evolution of ALS atrophy as recapitulated by network diffusion and evolved from the insula at model times $t = 2, 4, 6\ (au)$ is shown in Fig. 4. The evolution of network diffusion process seeded at the insula starts at early stage (t = 2) through mature stage (t = 6), where the maximum correspondence of NDM to empirical data occurred. Here, time is arbitrary, hence we have used "*au*" as the unit of time for illustrative purpose only. At the initial stage, the disease involves subcortical and frontal regions, followed by motor regions, and finally showing widespread involvement of extra-motor and cortical regions. A linear positive association between empirical atrophy and predicted atrophy $\left(\mathrm{R} = 0.45, \mathrm{p}_{\mathrm{corr}} < 5.8 \times 10^{-4}\right)$ as represented by the NDM at model times $t = 2, 4, 6\ (au)$ was demonstrated (Fig. 4B). A linear association was found between the histopathological staging and the NDM at model times $t = 2, 4, 6\ (au)$ (Fig. 4C), with a negative correlation between the predicted atrophy and stage, which as model time progresses, shows increased correlation between the NDM prediction from insula-seeding and each stage $\left(\mathrm{R} = -0.66, \mathrm{p}_{\mathrm{corr}} < 5.8 \times 10^{-4}\right)$. Earlier stages of histopathological staging show more atrophy compared to later stages, hence NDM predicted atrophy is negatively correlated with the histopathological stages at a given timepoint. Similarly, we also explored spatiotemporal evolution from thalamic-seeding at model times $t = 3, 5, 8\ (au)$ (Figure SI – 2). With thalamic-seeding, the predicted disease course involved mainly subcortical regions at the initial stage, followed by diffusion into the frontal and motor regions. P-values of

correlation between empirical and predicted atrophy for all model times are shown in Table SI – 4.

3.4. Relationship of atrophy to regional ALS risk gene expression

The linear relationship between different categories of genes (listed in Table SI – 5) and empirical atrophy was studied (Fig. 5). Fig. 5A shows distribution of empirical atrophy for reference. Fig. 5B and 5C show scatter plots of empirical atrophy versus averages of ALS-related genes, and TDP-43 specific genes respectively. No association was found between the average of ALS-related genes and TDP-43 specific genes with empirical atrophy. Further, no association was found between atrophy and TARTDP gene itself (Fig. 5D), which codes for TDP-43. Strong association with atrophy was found for a specific ALS-related and TDP- 43 specific gene: OPTN (R = 0.36) (Fig. 5E). The OPTN protein is a well- known etiological factor in ALS (Maruyama et al., 2010; Maruyama and Kawakami, 2013; Toth and Atkin, 2018; Feng et al., 2019). No other gene was significantly (after multiple comparisons correction) associated with empirical atrophy. Fig. 5F, 5G, 5H, and 5I show local distribution of average of ALS-related genes, average of TDP-43 specific genes, TARDBP, and OPTN, respectively. Table SI – 5 shows correlations of ALS-related genes, and their PCA vs. empirical atrophy (to the left) and correlations of TDP-43 specific genes and their PCA vs. empirical atrophy (to the right). These results suggest that genes alone do not contribute to regional vulnerability, and that linear association between atrophy and gene expression profiles are complex and cannot be explained by univariate analysis of genes alone.

3.5. NDM and regional ALS risk gene expression as joint predictors of atrophy

Although most ALS-implicated genes do not bear an association with regional atrophy directly, it is possible that they may contribute to regional atrophy along with network transmission of pathology. To test this, we used cross-validated L1 regularized regression (LASSO) feature selection to identify highly informative predictors of ALS pathology from the NDM and ALS-related genes, and those genes that might result in TDP-43 misfolding via downstream events. The model included the NDM predictor $\mathbf{x}_{tmax}^{In}$, 25 ALS-related genes, and 22 TDP-43 specific genes (Fig. 6). Two predictors survived lowest MSE plus one standard deviation (Lambda1SE) in our model, those highlighted and colored as seen in Fig. 6B, and were significant from multiple linear regression: $\mathbf{x}_{t\,max}^{In}$ * * and OPTN* with insula-seeding, suggesting that the NDM is the best predictor of ALS atrophy, and that only few genes in addition to the NDM contribute to the spatial pattern of disease, but in a weaker capacity.

Given that thalamic-seeding achieved the highest R from empirical data, LASSO analysis was repeated with NDM from thalamic-seeding using $\mathbf{x}_{t\,max}^{Th}$ and different categories of genes. With thalamic-seeding of NDM, two predictors survived: $\mathbf{x}_{tmax}^{Th}$ * * and OPTN*, (Figure SI – 3). However, again genes were far less significant contributors than NDM. Interestingly, the same gene most associated with regional atrophy – OPTN also survived LASSO with both insula and thalamus seeding. All other genes showed non-significant association with regional atrophy independent from NDM, suggesting that they do not significantly govern ALS topography. Interestingly, this is true even of those genes that are highly implicated in

ALS or involved with ALS pathology, e.g. TARDBP, MAPT or FUS. It may be that some of these genes are either collinear with NDM, or similar to OPTN.

3.6. NDM evaluation against alternate modeling of network connectivity and ALS atrophy

To test the predictive power of NDM against alternate network models, we evaluated its specificity to ALS atrophy and to the connectome upon which it evolves. The distribution of Pearson's R over 2000 randomly simulated connectome matrices and atrophy vectors from insula and thalamic-seeding are shown in Fig. 7 and Figure SI – 4 respectively. Random model's R was much lower than the maximum R of 0.45 from insula-seeding and 0.47 from thalamic-seeding which were achieved by the true model; statistically outside the 95% confidence interval, or $p < 0.05$. Hence, the reported insula and thalamic-seeded NDM outperforms all simulated models' prediction and is unlikely to be explained by chance.

4. Discussion

Using a quantitative network-based model of pathology spread, this study sought to explore selective vulnerability and pathological progression in the ALS brain. We tested whether, setting each region of our brain atlas as the initiation site, the subsequent network spread modeled by the NDM correctly and significantly recapitulates cross-sectional patterns of regional atrophy and *postmortem* pathology staging. We also incorporated a novel aspect involving the regional expression of ALS-related genes in the healthy brain. The results support structural network-based transmission in relation to regional atrophy, but with no consistent relationship to the spatial distribution of the regional expression of ALS-related genes. The identification of a specific gene associated significantly with atrophy – OPTN, within the network-gene interaction model (LASSO) using both insula- and thalamus-seeding, was a weaker but significant contributor in comparison to the NDM, and requires further dedicated study of this ALS genetic sub-group. No other gene showed significant association independently of NDM, including those involved in underlying pathology, but this may reflect the use of healthy brain regional expression data.

Intriguingly, the critical seed regions for spread within the model were not within the primary motor cortex but in basal ganglia, thalamus and insula. NDM applied to these seed regions also recapitulated the *postmortem* histopathological staging system. Within a continuous ALS-FTD clinicopathological spectrum, these non-primary motor structures may be the sites of some of the earliest cerebral pathology.

4.1. Stereotyped models of anatomical spread in ALS

The focality of initial symptom onset and the non-random, typically regionally contiguous spread of symptoms in ALS was shown to be mirrored, for limb involvement at least, by spinal cord histopathology (Ravits et al., 2007a,b). These data were used to infer a *theoretical* model of simultaneous cerebral focal onset and spread (Ravits and La Spada, 2009), but remain unproven. The most consistent regions of cerebral pathological involvement in ALS have been the corticospinal tract and corpus callosum (Filippini et al., 2010; Müller et al., 2016), but with wider extra-motor involvement at baseline and a variable extent of both gray and white matter changes in longitudinal studies (Menke et al., 2014).

Postmortem studies defined a variably overlapping extent of TDP-43 pathology, arbitrarily divided into four "stages", with presumed but as yet unproven sequential trans-axonal progression in vivo (Brettschneider et al., 2013). In that model initial lesions were said to develop in the agranular motor cortex, in the bulbar and spinal somatomotor neurons, and the brainstem motor nuclei (stage 1). The next affected regions were the prefrontal neocortex, the brainstem reticular formation, the pre-cerebellar nuclei, and the red nucleus (stage 2), then striatum and into the prefrontal/postcentral cortices (stage 3), finally involving anteromedial portions of the temporal lobe and the hippocampus (stage 4). This pathological staging has been supported by the same group in analysis of cross-sectional in vivo MRI data (Gorges et al., 2018).

4.2. Role of network transmission in ALS

A plausible explanation for these patterns of progression may be trans-neuronal transmission of underlying pathology, which has been hypothesized in other neurodegenerative disorders including Alzheimer's Disease, Frontotemporal Dementia (FTD), Parkinson's Disease, Huntington's Disease and Creutzfeldt–Jakob disease (Spillantini et al., 1998; Lee et al., 2001; Neumann et al., 2006; Hansen et al., 2011; Herrera et al., 2011; Jack and Holtzman, 2013; Jucker and Walker, 2013; Walker et al., 2013; Maniecka and Polymenidou, 2015; Freeze et al., 2020). Concepts of seeding and self-templating of aberrant, aggregate-prone proteins have extended to ALS (Polymenidou and Cleveland, 2011; Meier et al., 2020), with a similar hypothesis of trans-neuronal transmission of pathogenic proteins between cells (Schmidt et al., 2016; Subramaniam, 2019). These emerging concepts in ALS and FTD were comprehensively reviewed recently (Riku, 2020). Broader concepts of structural and functional networks in health have been invoked for defining patterns of neurodegeneration (Seeley et al., 2009). MRI studies in ALS have supported the concept that structural connectivity mediates the spatial and temporal evolution of ALS atrophy and leads to network disintegration (Verstraete et al., 2011, 2014; Schmidt et al., 2016; Bede et al., 2018; Törnquist et al., 2018; Meier et al., 2020).

The present study did not seek to investigate the question of whether structural connectivity networks themselves are being damaged by the disease process, but whether they might plausibly serve as conduits for regionally-preferential pathological transmission. We also explored alternate models of spread, principally whether proximity-based spread is capable of fitting empirical data – a widely assumed hypothesis. We found that the proximity model is not as well supported as the connectome-based model of spread.

A previous modeling study used a Gaussian resampling of the structural connectome and a random walker applied to the connectivity matrix directly to predict ALS disease progression (Meier et al., 2020). We chose not to impose any such transformation of the connectivity data and the NDM employed the graph Laplacian, which is an analytically closed form solution. In our study we allowed every possible region to serve as a potential starting point of the NDM as a regionally unbiased approach. Therefore our study used focal seeding sites per simulation, in comparison to using the entire histopathological stage I (Meier et al., 2020). Finally, and most importantly, our use of an atrophy measure of impairment from morphometric analysis, rather than a count of altered connections from

each graph node, is considered a more direct measure of neuronal loss, whereas the use of network alteration is considered a measure of loss of white matter projections.

4.3. Insula, basal ganglia and thalamus as potential seeding sites in ALS

The critical seed regions for widespread pathological spread within our model were not in the motor cortex but in basal ganglia, thalamus and insula. Furthermore, NDM applied to these seed regions recapitulated the *postmortem* TDP43-based histopathological staging scheme. These brain regions are well connected with prominent cortical areas undergoing atrophy in ALS (Bede et al., 2018). Basal ganglia involvement in ALS has been increasingly recognized (Bede et al., 2013; Riku, 2020) and the thalamus in particular has been shown to reflect the wider extent of cortical involvement in ALS (Chipika et al., 2020), notably in relation to the longitudinal spread of frontotemporal involvement (Tu et al., 2018).

A speculative interpretation of our results is that such sites may be common ‘anchors’ for what is a continuous ALS-FTD spectrum; see e.g. a recent review (Riku, 2020). The frontoinsula region appears to be one of the more selectively vulnerable and perhaps earliest sites of pathology in behavioral variant FTD, from which large von Economo neurons are prominently lost (Seeley et al., 2008; Kim et al., 2012). Similarly, the striatum is a site of early and prominent atrophy in bvFTD (Halabi et al.). Pathology in these non-primary motor deep gray matter structures may progress into either predominantly motor areas in ALS patients, or frontotemporal regions in FTD. Carriers of the intronic hexanucleotide expansion in *C9orf72*, the commonest inherited form of both ALS and FTD, tend to dichotomize into a phenotype with a predominance of one or other condition, even within the same pedigree (Mahoney et al., 2012), and the application of the methodology to a large cohort of such individuals might strengthen the hypothesis.

4.4. Limitations and future directions

The NDM is a first-order, linear model of diffusive spread that assumes that the structural connectivity network remains unchanged during disease course. Although all neurodegenerative diseases lead to aberrant structural connectivity, in practice normative connectomes as used here usually do not lead to significant reduction in the model’s predictive power (Powell et al, 2017). Individual subjects’ genetic variables, medication history and age of symptom onset were not analyzed. In this study we did not explore multi-seeding approach as implemented by (Poudel et al., 2020) as our study design requires an apples-to-apples comparison of seeding between subjects – a task that is very challenging statistically if there are varying degrees of freedom. A proper exploration of this concept will require a detailed and thoughtful inference algorithm that would need sparsity constraints, and a proper accommodation of degrees of freedom via AIC / BIC criteria. This approach did not fit within the current scope, and we hope to pursue it in a future study. Demonstrating the causality of gene variants in regional selective vulnerability is challenging and requires further modeling that also considers expression patterns seen in the disease state and in relation to specific genetic sub-groups e.g. *C9ORF72* expansion carriers. Furthermore, study of the association of the NDM with regional gene expression and atrophy considers only a narrow range of possible indexes of vulnerability. Correlation between model outcomes and clinical measures needs to fully be investigated

through prospective and longitudinal studies, especially those that focus explicitly on developing diagnostically predictive algorithms. In the increasing move toward prevention of neurodegenerative disorders through pre-symptomatic identification and intervention, this study further highlights the need to consider pathological changes disparate from those that define the symptomatic state.

Supplementary Material

Refer to Web version on PubMed Central for supplementary material.

Acknowledgments

Authors convey grateful thanks to Chris Mezias and Justin Torok at Weill-Cornell, and Pablo Damasceno at UCSF for help with network and gene analysis.

Funding

This study was supported by NIH grants NS092802 and R01AG062196 (to AR). MRT was supported by the Medical Research Council & Motor Neurone Disease Association Lady Edith Wolfson Fellowships (G0701923 & MR/K01014X/1) and the Motor Neurone Disease Association Walker Professorship.

Data availability

All data used in this study will be made available upon reasonable request and relevant code will be uploaded to https://github.com/Raj-Lab-UCSF repository. Oxford's Wellcome center for Integrative Neuroimaging has an inherent commitment to data-sharing. To get access to the data and comply with the research ethics committee approval an application to the corresponding author will be required so that the precise geographical extent of sharing is known.

References

Agosta F, Chiò A, Cosottini M, De Stefano N, Falini A, Mascalchi M, et al. , 2010. The present and the future of neuroimaging in amyotrophic lateral sclerosis. Am. J. Neuroradiol 31, 1769–1777. [PubMed: 20360339]

Arnatkeviciute A, Fulcher BD, Fornito A, 2019. A practical guide to linking brain-wide gene expression and neuroimaging data. Neuroimage 189, 353–367. [PubMed: 30648605]

Bede P, Elamin M, Byrne S, McLaughlin RL, Kenna K, Vajda A, et al. , 2013. Basal ganglia involvement in amyotrophic lateral sclerosis. Neurology 81, 2107–2115. [PubMed: 24212388]

Bede P, Omer T, Finegan E, Chipika RH, Iyer PM, Doherty MA, et al. , 2018. Connectivity-based characterisation of subcortical grey matter pathology in frontotemporal dementia and ALS: a multimodal neuroimaging study. Brain Imaging Behav 12, 1696–1707. [PubMed: 29423814]

Braak H, Brettschneider J, Ludolph AC, Lee VM, Trojanowski JQ, Del, Tredici K, 2013. Amyotrophic lateral sclerosis —a model of corticofugal axonal spread. Nat. Rev. Neurol 9, 708–714. [PubMed: 24217521]

Braak H, Neumann M, Ludolph A, Del Tredici K, 2017. Does sporadic amyotrophic lateral sclerosis spread via axonal connectivities? Neurol. Int. Open 01, E136–E141.

Braak H, Del Tredici K, 2018. Anterior cingulate cortex TDP-43 pathology in sporadic amyotrophic lateral sclerosis. J. Neuropathol. Exp. Neurol 77, 74–83. [PubMed: 29186496]

Brettschneider J, Del Tredici K, Toledo JB, Robinson JL, Irwin DJ, Grossman M, et al. , 2013. Stages of pTDP-43 pathology in amyotrophic lateral sclerosis. Ann. Neurol 74, 20–38. [PubMed: 23686809]

Chia R, Chiò A, Traynor BJ., 2018. Novel genes associated with amyotrophic lateral sclerosis: diagnostic and clinical implications. Lancet. Neurol 17, 94–102. [PubMed: 29154141]

Chiò A, Pagani M, Agosta F, Calvo A, Cistaro A, Filippi M, 2014. Neuroimaging in amyotrophic lateral sclerosis: insights into structural and functional changes. Lancet. Neurol 13, 1228–1240. [PubMed: 25453462]

Chipika RH, Finegan E, Li Hi Shing S, McKenna MC, Christidi F, Ming Chang K, et al. , 2020. Switchboard ” malfunction in motor neuron diseases: selective pathology of thalamic nuclei in amyotrophic lateral sclerosis and primary lateral sclerosis. NeuroImage Clin, 102300. [PubMed: 32554322]

Cykowski MD, Takei H, Schulz PE, Appel SH, Powell SZ., 2014. TDP-43 pathology in the basal forebrain and hypothalamus of patients with amyotrophic lateral sclerosis. Acta Neuropathol. Commun 2, 171. [PubMed: 25539830]

Es M van, Hardiman O, Chio A, Al-Chalabi A, Pasterkamp RJ, Veldink JJH, et al. , 2017. Amyotrophic lateral sclerosis. Lancet 390, 2084–2098. [PubMed: 28552366]

Feng S, Che C, Feng S, Liu C, Li L, Li Y, et al. , 2019. Novel mutation in optineurin causing aggressive ALS +/− frontotemporal dementia. Ann. Clin. Transl. Neurol 6, 2377–2383. [PubMed: 31838784]

Filippini N, Douaud G, Mackay CE, Knight S, Talbot K, Turner MR., 2010. Corpus callosum involvement is a consistent feature of amyotrophic lateral sclerosis. Neurology 75, 1645–1652. [PubMed: 21041787]

Freeze B, Acosta D, Pandya S, Zhao Y, Raj A, 2018. Regional expression of genes mediating trans-synaptic alpha-synuclein transfer predicts regional atrophy in Parkinson disease. NeuroImage Clin 18, 456–466. [PubMed: 29868450]

Freeze B, Maia P, Pandya S, Raj A, 2020. Network mediation of pathology pattern in sporadic Creutzfeldt-Jakob disease. Brain Commun.

Freeze B, Pandya S, Zeighami Y, Raj A, 2019. Regional transcriptional architecture of Parkinson’s disease pathogenesis and network spread. Brain 142, 3072–3085. [PubMed: 31359041]

Fusco FR, Chen Q, Lamoreaux WJ, Figueredo-Cardenas G, Jiao Y, Coffman JA, et al. , 1999. Cellular localization of huntingtin in striatal and cortical neurons in rats: Lack of correlation with neuronal vulnerability in Huntington’s disease. J. Neurosci 19, 1189–1202. [PubMed: 9952397]

Gorges M, Del Tredici K, Dreyhaupt J, Braak H, Ludolph AC, Müller H-P, et al. , 2018. Corticoefferent pathology distribution in amyotrophic lateral sclerosis: in vivo evidence from a meta-analysis of diffusion tensor imaging data. Sci. Rep 8, 15389. [PubMed: 30337677]

Grosskreutz J, Kaufmann J, Frädrich J, Dengler R, Heinze H-J, Peschel T, 2006. Widespread sensorimotor and frontal cortical atrophy in Amyotrophic Lateral Sclerosis. BMC Neurol 6, 17. [PubMed: 16638121]

Halabi C, Halabi A, Dean DL, Wang P-N, Boxer AL, Trojanowski JQ, et al. Patterns of striatal degeneration in frontotemporal dementia. Alzheimer Dis. Assoc. Disord; 27: 74–83. [PubMed: 22367382]

Hansen C, Angot E, Bergström A-L, Steiner JA, Pieri L, Paul G, et al. , 2011. α-Synuclein propagates from mouse brain to grafted dopaminergic neurons and seeds aggregation in cultured human cells. J. Clin. Invest 121, 715–725. [PubMed: 21245577]

Hawrylycz MJ, Lein ES, Guillozet-Bongaarts AL, Shen EH, Ng L, Miller JA, et al. , 2012. An anatomically comprehensive atlas of the adult human brain transcriptome. Nature 489, 391–399. [PubMed: 22996553]

Herrera F, Tenreiro S, Miller-Fleming L, Outeiro TF., 2011. Visualization of cell-to-cell transmission of mutant huntingtin oligomers. PLoS Curr.

Iturria-Medina Y, Canales-Rodríguez EJ, Melie-García L, Valdés-Hernández PA, Martínez-Montes E, Alemán-Gómez Y, et al. , 2007. Characterizing brain anatomical connections using diffusion weighted MRI and graph theory. Neuroimage 36, 645–660. [PubMed: 17466539]

Jack CR, Holtzman DM., 2013. Biomarker modeling of Alzheimer’s disease. Neuron 80, 1347–1358. [PubMed: 24360540]

Jackson WS., 2014. Selective vulnerability to neurodegenerative disease: the curious case of prion protein. DMM Dis. Model. Mech 7, 21–29. [PubMed: 24396151]

Jucker M, Walker LC., 2013. Self-propagation of pathogenic protein aggregates in neurodegenerative diseases. Nature 501, 45–51. [PubMed: 24005412]

Karch CM, Wen N, Fan CC, Yokoyama JS, Kouri N, Ross OA, et al. , 2018. Selective genetic overlap between amyotrophic lateral sclerosis and diseases of the frontotemporal dementia spectrum. JAMA Neurol 75, 860–875. [PubMed: 29630712]

Kassubek J, Unrath A, Huppertz H, Lulé D, Ethofer T, Sperfeld A, et al. , 2005. Global brain atrophy and corticospinal tract alterations in ALS, as investigated by voxel-based morphometry of 3-D MRI. Amyotroph. Lateral Scler. 6, 213–220.

Kawakami I, Arai T, Hasegawa M, 2019. The basis of clinicopathological heterogeneity in TDP-43 proteinopathy. Acta Neuropathol 138, 751–770. [PubMed: 31555895]

Kim E-J, Sidhu M, Gaus SE, Huang EJ, Hof PR, Miller BL, et al. , 2012. Selective frontoinsular von Economo neuron and fork cell loss in early behavioral variant frontotemporal dementia. Cereb. Cortex 22, 251–259. [PubMed: 21653702]

Kuceyeski A, Maruta J, Relkin N, Raj A, 2013. The Network Modification (NeMo) Tool: elucidating the effect of white matter integrity changes on cortical and subcortical structural connectivity. Brain Connect 3, 451–463. [PubMed: 23855491]

Lee VM-Y, Goedert M, 2001. Trojanowski JQ. neurodegenerative tauopathies. Annu. Rev. Neurosci 24, 1121–1159. [PubMed: 11520930]

LoCastro E, Kuceyeski A, Raj A, 2014. Brainography: an atlas-independent surface and network rendering tool for neural connectivity visualization. Neuroinformatics 12, 355–359. [PubMed: 24081830]

Mahoney CJ, Beck J, Rohrer JD, Lashley T, Mok K, Shakespeare T, et al. , 2012. Frontotemporal dementia with the C9ORF72 hexanucleotide repeat expansion: clinical, neuroanatomical and neuropathological features. Brain 135, 736–750. [PubMed: 22366791]

Maniecka Z, Polymenidou M, 2015. From nucleation to widespread propagation: a prion-like concept for ALS. Virus Res 207, 94–105. [PubMed: 25656065]

Marinescu RV, Eshaghi A, Alexander DC, Golland P, 2019. BrainPainter: a software for the visualisation of brain structures. Biomark. Assoc. Pathol. Process 112–120.

Markello RD, Arnatkeviciute A, Poline J-B, Fulcher BD, Fornito A, Misic B, 2021. Standardizing workflows in imaging transcriptomics with the abagen toolbox [Internet]. Elife 10. Available from: https://elifesciences.org/articles/72129.

Maruyama H, Kawakami H, 2013. Optineurin and amyotrophic lateral sclerosis. Geriatr. Gerontol. Int 13, 528–532. [PubMed: 23279185]

Maruyama H, Morino H, Ito H, Izumi Y, Kato H, Watanabe Y, et al. , 2010. Mutations of optineurin in amyotrophic lateral sclerosis. Nature 465, 223–226. [PubMed: 20428114]

Meier JM, van der Burgh HK, Nitert AD, Bede P, de Lange SC, Hardiman O, et al. , 2020. Connectome-based propagation model in amyotrophic lateral sclerosis. Ann. Neurol 87, 725–738. [PubMed: 32072667]

Menke RAL, Agosta F, Grosskreutz J, Filippi M, Turner MR., 2017. Neuroimaging endpoints in amyotrophic lateral sclerosis. Neurotherapeutics 14, 11–23. [PubMed: 27752938]

Menke RAL, Körner S, Filippini N, Douaud G, Knight S, Talbot K, et al. , 2014. Widespread grey matter pathology dominates the longitudinal cerebral MRI and clinical landscape of amyotrophic lateral sclerosis. Brain 137, 2546–2555. [PubMed: 24951638]

Menke RAL, Proudfoot M, Talbot K, Turner MR, 2018. The two-year progression of structural and functional cerebral MRI in amyotrophic lateral sclerosis. NeuroImage Clin 17, 953–961. [PubMed: 29321969]

Mezzapesa DM, Ceccarelli A, Dicuonzo F, Carella A, De Caro MF, Lopez M, et al. , 2007. Whole-brain and regional brain atrophy in amyotrophic lateral sclerosis. AJNR. Am. J. Neuroradiol 28, 255–259. [PubMed: 17296989]

Müller H-P, Turner MR, Grosskreutz J, Abrahams S, Bede P, Govind V, et al. , 2016. A large-scale multicentre cerebral diffusion tensor imaging study in amyotrophic lateral sclerosis. J. Neurol. Neurosurg. Psychiatry 87, 570–579. [PubMed: 26746186]

Neumann M, Sampathu DM, Kwong LK, Truax AC, Micsenyi MC, Chou TT, et al. , 2006. Ubiquitinated TDP-43 in frontotemporal lobar degeneration and amyotrophic lateral sclerosis. Science (80-.) 314, 130–133. [PubMed: 17023659]

Nicolas A, Kenna KP, Renton AE, Ticozzi N, Faghri F, Chia R, et al. , 2018. Genome-wide analyses identify KIF5A as a novel ALS gene. Neuron 97, 1268–1283 e6. [PubMed: 29566793]

Pandya S, Mezias C, Raj A, 2017. Predictive model of spread of progressive supranuclear palsy using directional network diffusion. Front. Neurol 8.

Pandya S, Zeighami Y, Freeze B, Dadar M, Collins DL, Dagher A, et al. , 2019. Predictive model of spread of Parkinson's pathology using network diffusion. Neuroimage 192, 178–194. [PubMed: 30851444]

Philips T, Rothstein JD., 2014. Glial cells in amyotrophic lateral sclerosis. Exp. Neurol 262, 111–120. [PubMed: 24859452]

Polymenidou M, Cleveland DW., 2011. The seeds of neurodegeneration: prion-like spreading in ALS. Cell 147, 498–508. [PubMed: 22036560]

Poudel GR, Dominguez DJF, Verhelst H, Vander Linden C, Deblaere K, Jones DK, et al. , 2020. Network diffusion modeling predicts neurodegeneration in traumatic brain injury. Ann. Clin. Transl. Neurol 7, 270–279. [PubMed: 32105414]

Poudel GR, Harding IH, Egan GF, 2019. Georgiou-Karistianis N. Network spread determines severity of degeneration and disconnection in Huntington's disease. Hum. Brain Mapp 40, 4192–4201. [PubMed: 31187915]

Proudfoot M, Menke RAL, Sharma R, Berna CM, Hicks SL, Kennard C, et al. , 2015. Eye-tracking in amyotrophic lateral sclerosis: A longitudinal study of saccadic and cognitive tasks. Amyotroph. Lateral Scler. Frontotemporal Degener. 17, 101–111. [PubMed: 26312652]

Raj A, Kuceyeski A, Weiner M, 2012. A network diffusion model of disease progression in dementia. Neuron.

Raj A, LoCastro E, Kuceyeski A, Tosun D, Relkin N, Weiner M, 2015. Network diffusion model of progression predicts longitudinal patterns of atrophy and metabolism in Alzheimer's. Disease. Cell Rep 10, 359–369. [PubMed: 25600871]

Ravits J, Laurie P, Fan Y, Moore DH, 2007a. Implications of ALS focality: rostral-caudal distribution of lower motor neuron loss postmortem. Neurology 68, 1576–1582. [PubMed: 17485644]

Ravits J, Paul P, Jorg C, 2007b. Focality of upper and lower motor neuron degeneration at the clinical onset of ALS. Neurology 68, 1571–1575. [PubMed: 17485643]

Ravits JM, La Spada AR, 2009. ALS motor phenotype heterogeneity, focality, and spread: deconstructing motor neuron degeneration. Neurology 73, 805–811. [PubMed: 19738176]

Riku Y, 2020. Reappraisal of the anatomical spreading and propagation hypothesis about TDP-43 aggregation in amyotrophic lateral sclerosis and frontotemporal lobar degeneration. Neuropathology. Blackwell Publishing

Robberecht W, Eykens C, 2015. The genetic basis of amyotrophic lateral sclerosis: recent breakthroughs. Adv. Genomics Genet 5, 327.

Schmidt R, de Reus MA, Scholtens LH, van den Berg LH, van den Heuvel MP., 2016. Simulating disease propagation across white matter connectome reveals anatomical substrate for neuropathology staging in amyotrophic lateral sclerosis. Neuroimage 124, 762–769. [PubMed: 25869856]

Scotter EL, Chen H-J, Shaw CE, 2015. TDP-43 proteinopathy and ALS: insights into disease mechanisms and therapeutic targets. Neurotherapeutics 12, 352–363. [PubMed: 25652699]

Seeley WW, Crawford R, Rascovsky K, Kramer JH, Weiner M, Miller BL, et al. , 2008. Frontal paralimbic network atrophy in very mild behavioral variant frontotemporal dementia. Arch. Neurol 65, 249–255. [PubMed: 18268196]

Seeley WW, Crawford RK, Zhou J, Miller BL, Greicius MD., 2009. Neurodegenerative diseases target large-scale human brain networks. Neuron 62, 42–52. [PubMed: 19376066]

Smith BN, Topp SD, Fallini C, Shibata H, Chen H-J, Troakes, C, et al. , 2017. Mutations in the vesicular trafficking protein annexin A11 are associated with amyotrophic lateral sclerosis. Sci. Transl. Med 9.

Spillantini MG, Crowther RA, Jakes R, Hasegawa M, 1998. Goedert M. α-Synuclein in filamentous inclusions of Lewy bodies from Parkinson's disease and dementia with Lewy bodies. Proc. Natl. Acad. Sci. U. S. A 95, 6469–6473. [PubMed: 9600990]

Subramaniam S, 2019. Selective neuronal death in neurodegenerative diseases: the ongoing mystery. Yale J. Biol. Med 92, 695–705. [PubMed: 31866784]

Talbot K, Feneberg E, Scaber J, Thompson AG, Turner MR., 2018. Amyotrophic lateral sclerosis: the complex path to precision medicine. J. Neurol 265, 2454–2462. [PubMed: 30054789]

Törnquist M, Michaels TCT, Sanagavarapu K, Yang X, Meisl G, Cohen SIA, et al. , 2018. Secondary nucleation in amyloid formation. Chem. Commun 54, 8667–8684.

Toth RP, Atkin JD., 2018. Dysfunction of optineurin in amyotrophic lateral sclerosis and glaucoma. Front. Immunol 9, 1017. [PubMed: 29875767]

Tu S, Menke RAL, Talbot K, Kiernan MC, Turner MR., 2018. Regional thalamic MRI as a marker of widespread cortical pathology and progressive frontotemporal involvement in amyotrophic lateral sclerosis. J. Neurol. Neurosurg. Psychiatry 89, 1250–1258. [PubMed: 30049750]

Turner MR, Bowser R, Bruijn L, Dupuis L, Ludolph A, McGrath M, et al. , 2013. Mechanisms, models and biomarkers in amyotrophic lateral sclerosis. Amyotroph. Lateral Scler. Front. Degener 14, 19–32.

Turner MR, Brockington A, Scaber J, Hollinger H, Marsden R, Shaw PJ, et al. , 2010. Pattern of spread and prognosis in lower limb-onset ALS. Amyotroph. Lateral Scler 11, 369–373. [PubMed: 20001488]

Turner MR, Swash M, 2015. The expanding syndrome of amyotrophic lateral sclerosis: a clinical and molecular odyssey. J. Neurol. Neurosurg. Psychiatry 86, 667–673. [PubMed: 25644224]

Vajda A, McLaughlin RL, Heverin M, Thorpe O, Abrahams S, Al-Chalabi A, et al. , 2017. Genetic testing in ALS: A survey of current practices. Neurology 88, 991–999. [PubMed: 28159885]

Verstraete E, Veldink JH, van den Berg LH, Van den Heuvel MP., 2014. Structural brain network imaging shows expanding disconnection of the motor system in amyotrophic lateral sclerosis. Hum. Brain Mapp 35, 1351–1361. [PubMed: 23450820]

Verstraete E, Veldink JH, Mandl RC, van den Berg LH, van den Heuvel MP., 2011. Impaired structural motor connectome in amyotrophic lateral sclerosis. PLoS One 6, e24239. [PubMed: 21912680]

Walker LC, Diamond MI, Duff KE, Hyman BT., 2013. Mechanisms of protein seeding in neurodegenerative diseases. JAMA Neurol. 70, 304–310. [PubMed: 23599928]

Westeneng H-J, Verstraete E, Walhout R, Schmidt R, Hendrikse, Veldink JH, et al. , 2015. Subcortical structures in amyotrophic lateral sclerosis. Neurobiol. Aging 36, 1075–1082. [PubMed: 25281019]

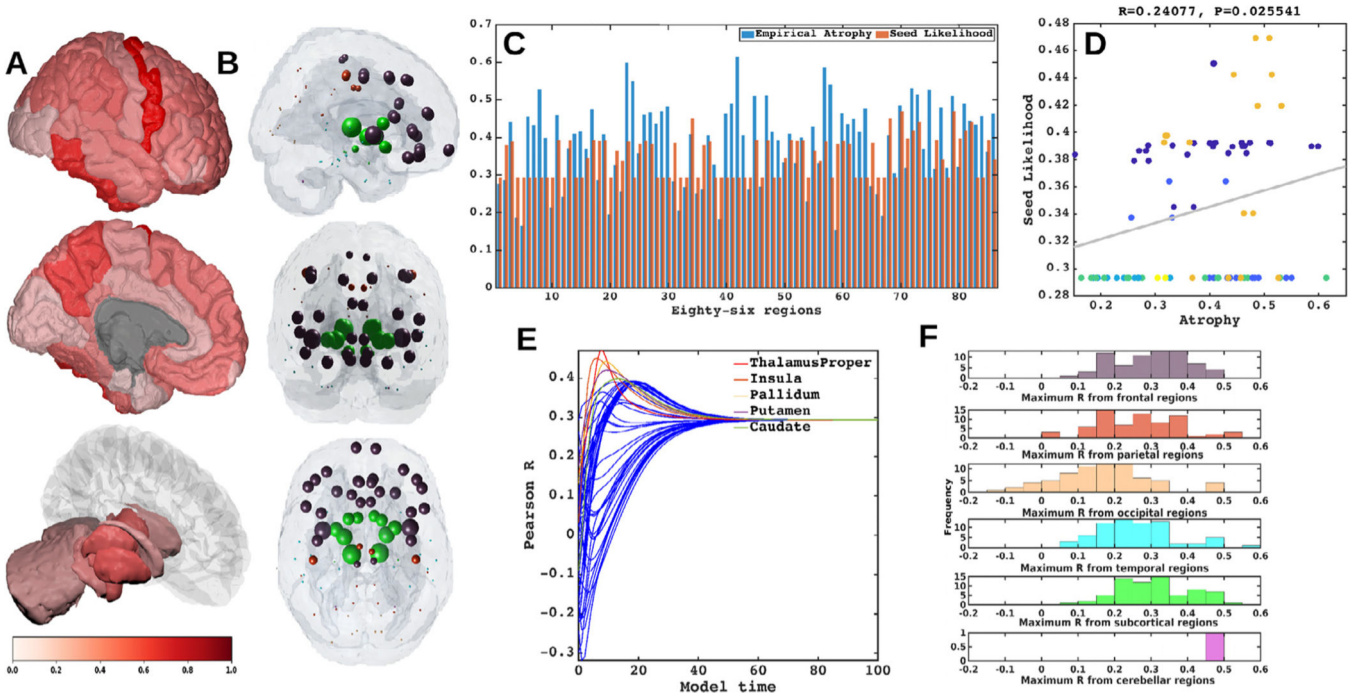

Fig. 1. Spatial distribution of ALS atrophy and repeated seeding.

A] Measured regional ALS atrophy are depicted by glass brain visualization. Bilateral volume loss was observed in somatosensory, frontotemporal, and subcortical regions, with most atrophy occurring in precentral gyrus, inferior temporal gyrus, precuneus, putamen, and thalamus regions. Severity of disease in each region is depicted in a color bar, where color towards red show increased severity. B] Each region was seeded in turn and NDM was played out for all time points. Pearson's R was recorded at each time point between the model and ALS atrophy vector. As the diffusion time increases, more and more of the pathogenic agent escapes the seed region and enters the rest of the network. The point of maximum correlation with measured atrophy was recorded with glass brains of measured R shown inset. Spheres are placed at the centroid of each brain region, and their diameter is proportional to effect size. Spheres are color coded by lobe – frontal = purple, parietal = red, occipital = orange, temporal = cyan, subcortical = green, and cerebellum = magenta. C] Histogram of empirical atrophy and seed region likelihood as represented by R_{max} is shown side-by-side. Precentral which is the highest atrophied region when taking the average of empirical atrophy from left hemisphere (LH) and right hemisphere (RH) is not the best seed, thereby suggestive of inconsequential role of higher atrophy values in determination of R_{max}. D] Scatter plot of empirical atrophy and seed region likelihood (represented as R_{max}) showing a weak relationship between the two, thereby suggesting a non-trivial role played by empirical atrophy in reproducing R_{max}. E] NDM seeded at bilateral regions indicates that the thalamus is the one of the most plausible candidate for ALS seeding – it has the highest peak R, and the characteristic intermediate peak indicative of true pathology spread. Other regions among the top five that obtained the highest R were insula, pallidum, putamen, and caudate. R-t curves for the remaining regions are shown in blue. F] Histogram of maximum R achieved from six major regions for all individual subjects. R_{max} values were attained for each of these regions from 79 individual subjects. We can see that for most of the subjects'

maximum R (> 0.4) was achieved from the frontal and subcortical regions compared to other regions.

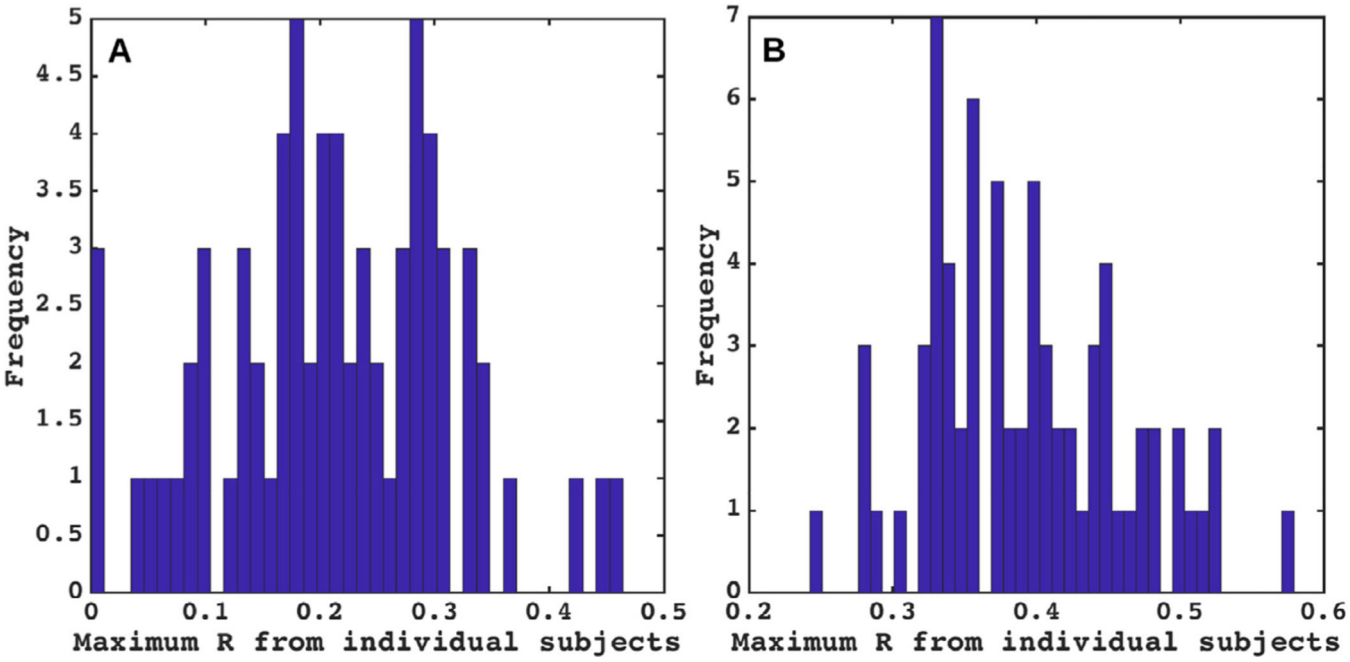

Fig. 2. Histogram of R_{max} from individual subjects.

A] Distribution of R_{max} for individual subjects when NDM is ran from insula seeding. B] Distribution of R_{max} for individual subjects when NDM is ran from their best seeds.

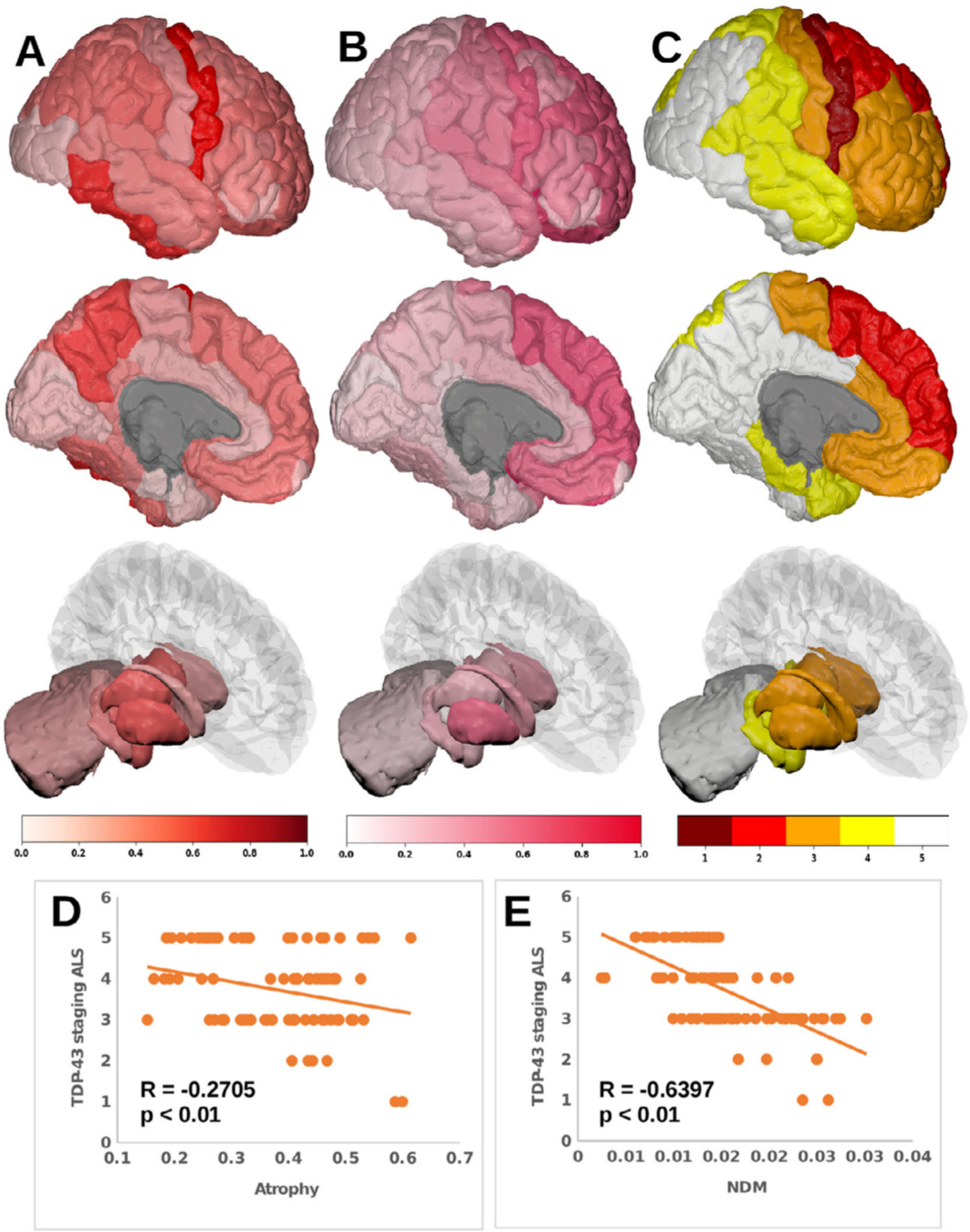

Fig. 3. Spatial distribution of ALS atrophy, NDM Predicted atrophy and histopathological staging.

A] Measured regional ALS atrophy are depicted by glass brain visualization. Bilateral volume loss was observed in somatosensory, frontotemporal, and subcortical regions, with most atrophy occurring in precentral gyrus, inferior temporal gyrus, precuneus, putamen, and thalamic regions. Severity of disease in each region is depicted in a color bar, where color towards red show increased severity. B] Glass brains of NDM seeded at the bilateral insula at t_{max} = 6.06 au yields progression of ALS from insula to connected, subcortical,

anteromedial portions of temporal lobe and frontal areas. Bilateral volume loss is mainly observed in frontal and subcortical regions, with most atrophy occurring in later orbito-frontal, superior frontal, precentral, rostral middle-frontal, and putamen regions. Severity of disease in each region is depicted in a color bar, where color towards magenta showing increased severity. C] The ALS stage from 1–4 for each of the 43 bilateral regions. Stage 1 (maroon) starts with agranular motor cortex. The next affected regions (stage 2 in red) are the premotor cortex and parts of prefrontal neocortex. The pathology then progresses into striatum and into the prefrontal/postcentral cortices (stage 3 in orange), and finally to stage 4 show (yellow) involving anteromedial portions of the temporal lobe and the hippocampus. Stage 5 shows regions in white that are not part of the published histopathological staging system. D] Correlation of empirical atrophy with histopathological staging. E] Correlation of NDM at t_{max} = 6.06 au with histopathological staging. Scatter plots in both D and E shows that regions with more empirical and predicted pathology correspond to histological stages with severe TDP-43 burden.

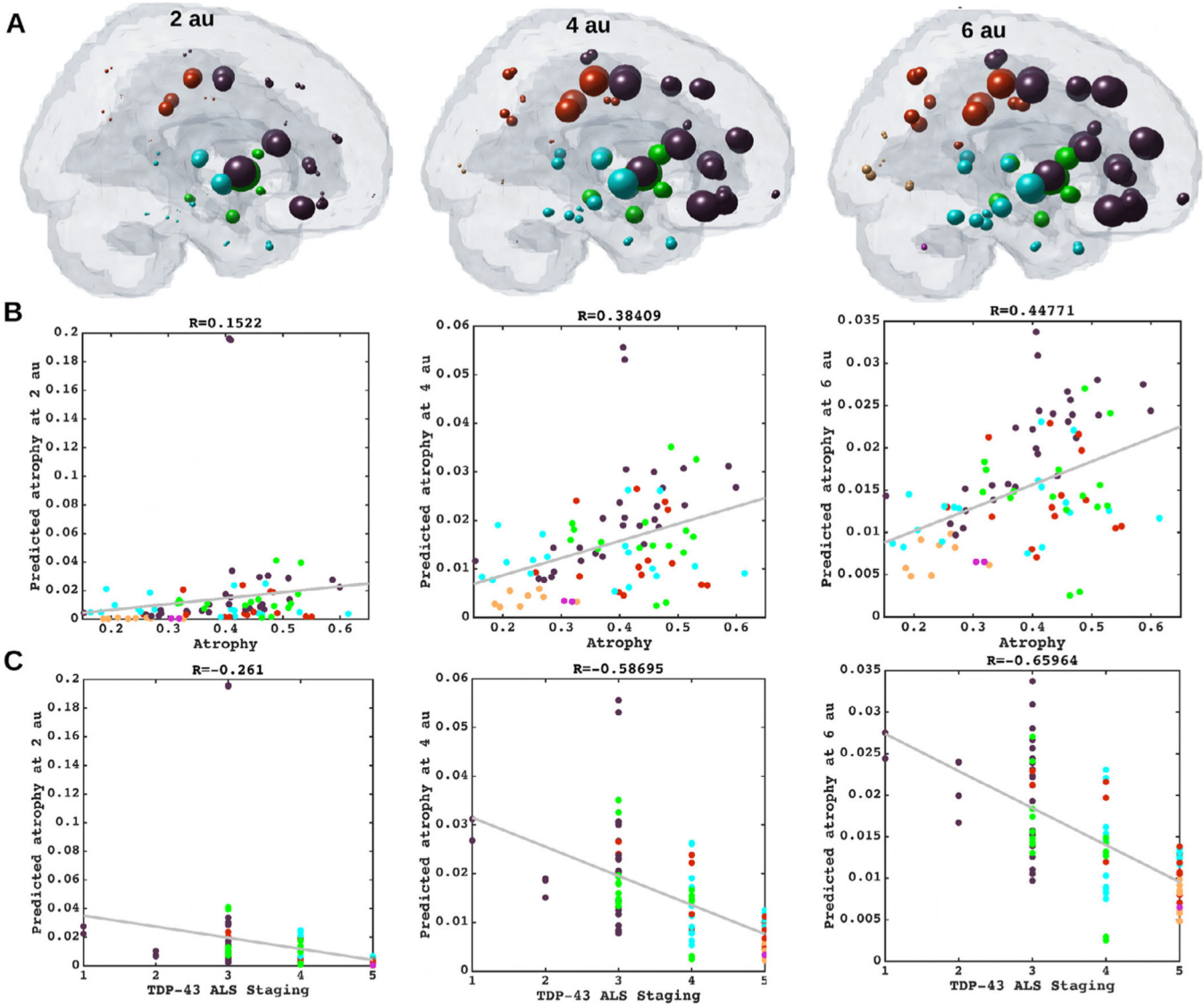

Fig. 4. Spatiotemporal evolution, scatter plots of atrophy and histopathological staging with NDM at different model times.

A] Evolution of insula-seeded network diffusion at model times $t = 2, 4, 6$ (au) exhibited frontal involvement initially, followed by slower diffusion into the temporal, motor, and subcortical cortices, and finally showing widespread involvement of cortical regions. This temporal sequencing predicted by the model suggests that volume loss in ALS involves extra-motor regions, particularly the prefrontal and subcortical regions. Nodes in all the glass brains are placed at the centroid of each brain region, and their diameter is proportional to effect size. Spheres are color coded by lobe – frontal = purple, parietal = red, occipital = orange, temporal = cyan, subcortical = green, and cerebellum = magenta. B] Scatter plot of NDM from insula versus empirical ALS atrophy at model times $t = 2, 4, 6$ (au). Dots are color coded by lobe - frontal = purple; parietal = red; occipital = orange; temporal = cyan; subcortical = green; and cerebellum = magenta. A positive correlation is observed between ALS empirical atrophy and NDM predicted atrophy from bilateral insula,

which increases significantly (R = 0.45, $p_{corr} < 5.8 \times 10^{-4}$, 0.05/86) at matured model times $t = 4, 6$ (*au*). C] Scatter plot of NDM from insula versus histopathological staging at model times $t = 2, 4, 6$ (*au*). Dots are color coded by lobe - frontal = purple; parietal = red; occipital = orange; temporal = cyan; subcortical = green; and cerebellum = magenta. A negative correlation was observed between the NDM and ALS staging from bilateral insula, which decreases significantly (R = −0.66, $p_{corr} < 5.8 \times 10^{-4}$) at matured model times $t = 4, 6$ (*au*). As time progressed, greater frontal, temporal and subcortical regions were involved with NDM closely resembling empirical ALS-FTD pathology.

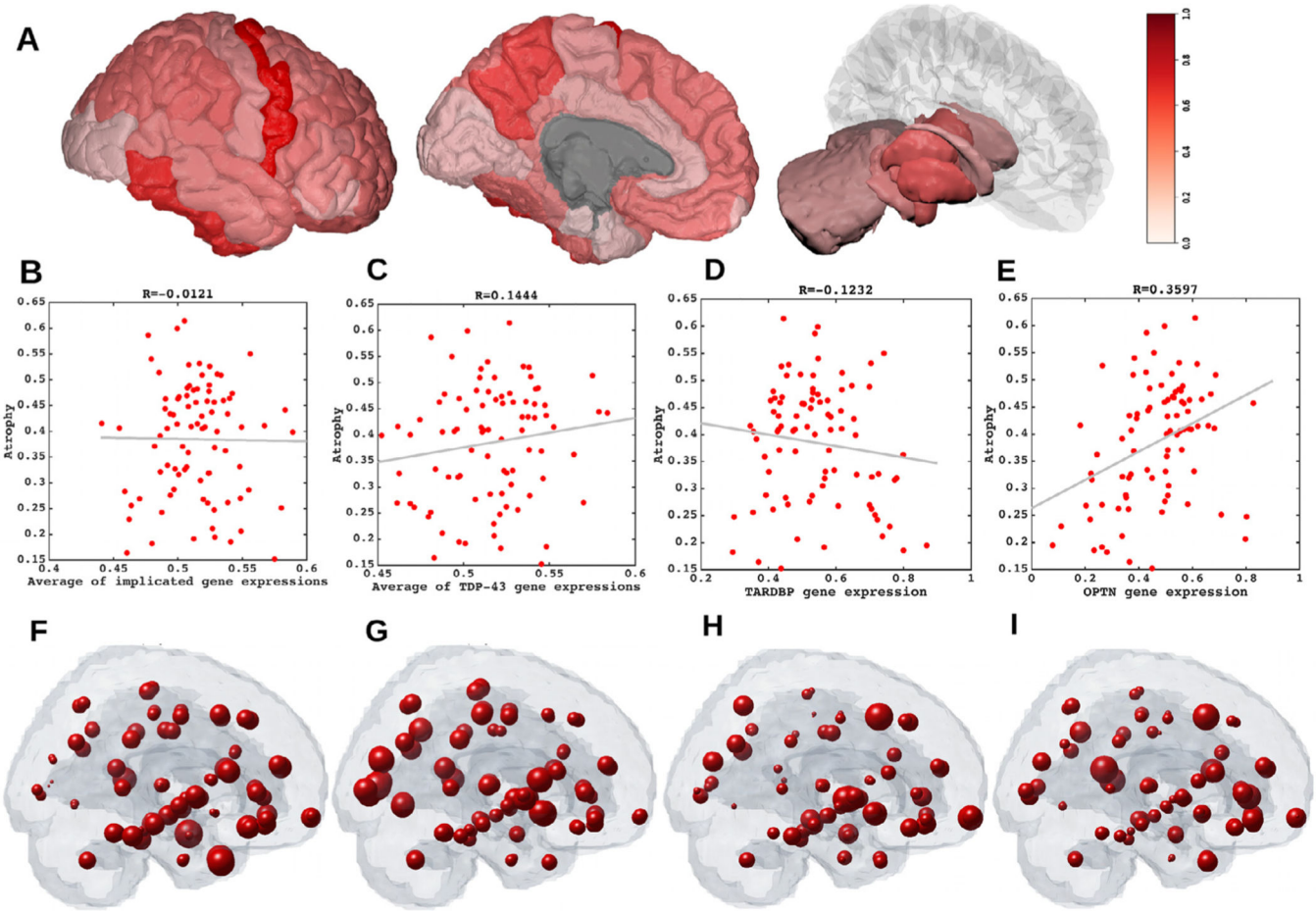

Fig. 5. Spatial distribution of ALS atrophy, scatter plots of genes vs ALS atrophy, spatial distribution of genes.

A] Measured regional ALS atrophy are depicted by glass brain visualization. Bilateral volume loss was observed in somatosensory, frontotemporal, and subcortical regions, with most atrophy occurring in precentral gyrus, inferior temporal gyrus, precuneus, putamen, and thalamic regions. Severity of disease in each region is depicted in a color bar, where color towards red show increased severity. B] Scatter plot of empirical atrophy vs average of all ALS-related genes (F) shows no clear association. C] Scatter plot of empirical atrophy vs average of TDP-43 associated genes (G) shows no clear association. D] Scatter plot of empirical atrophy vs TARDBP gene expression (H) also shows no clear association – this was chosen for comparison, given that a small minority of ALS cases involve mutations in TARDBP. E] Scatter plot of empirical atrophy vs OPTN gene expression (I) shows a strong association between them – this is shown for comparison given a strong correlation between the two. Spheres in glass brains were placed at the centroid of each brain region, and their diameter was proportional to effect size.

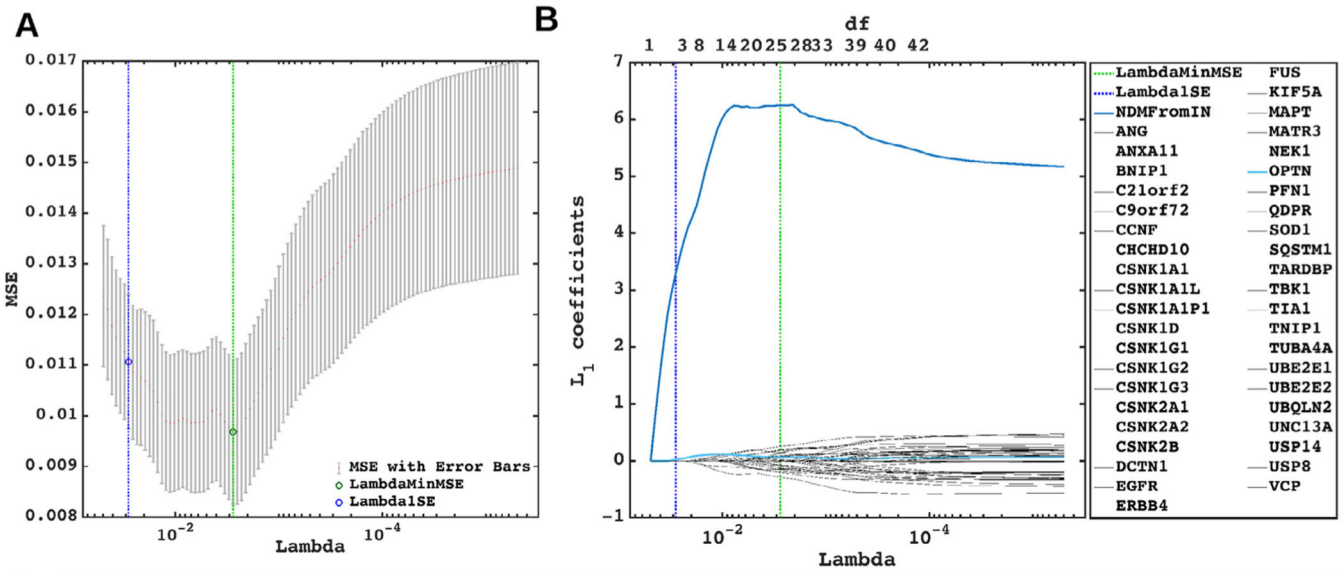

C

Region Names	Estimate	SE	tstat	p-val
NDM	6.72	1.89	3.56	6.17×10^{-04} **
OPTN	0.16	0.07	2.14	0.04 *

** $p_{corr} < 0.001$; * $p < 0.05$

Fig. 6. Lasso plots and model parameters from insula-seeding.

A] Cross-validated MSE curves for determining regularized parameter lambda. Predictors with minimum L1 coefficient as a function of regularized parameter lambda with no more than one standard deviation (blue dotted line) were considered to be the most favorable. B] Cross-validated L_1 regularized regression coefficients as a function of tuning parameter lambda for a model containing the NDM from insula, ALS-related genes, and genes implicated in trans-synaptic TDP-43 transfer as predictors. Trace plot shows that as lambda increases towards the left, lasso sets various coefficients to zero, thereby removing them from the model. C] Model parameters and p-values of significant predictors from multiple linear regression that survived with $p < 0.05$ (represented with "*") and with Bonferroni corrected p (represented with "**"). The NDM and expression profiles of OPTN have non-zero coefficients at Lambda1SE and were significant, indicating that these are essential predictive variables.

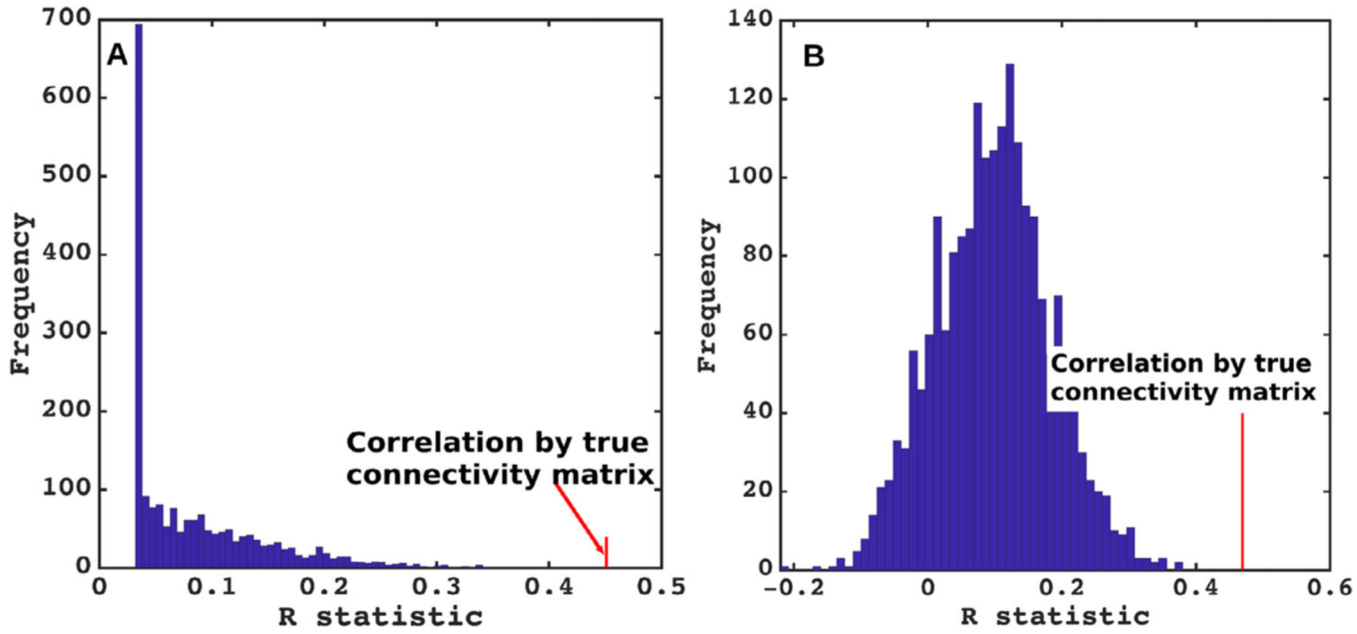

Fig. 7. NDM evaluation against alternate models.

A] Histogram of correlation strength between NDM and ALS data over 2000 shuffled networks. There is a hard limit on the left of this plot at R ~0.03, which corresponds to the zero-diffusion time value of curve in Fig. 1E. B] Histogram of correlation strength between NDM and 2000 shuffled ALS data over using unshuffled structural connectome. The true connectome was shuffled by symmetrically permuting its rows and columns randomly, and the NDM was evaluated for each shuffled network after bilateral insula-seeding. The best R achieved by each model was recorded and entered into the histogram. The null models are distributed well below the true model, indicating that the latter is highly unlikely to arise by chance ($p < 0.05$).

Table 1

List of regions most likely to serve as seeds of ALS pathology. Seeding likelihood of a region, shown in the rightmost column, is denoted by the average of the highest R from both empirical atrophy and histopathological staging. Although the precentral gyrus does not have the highest seeding likelihood by these measures, it was included here due to its prominence as an early site in ALS.

Region	Atrophy	R_{max} (NDM vs Atrophy)	R_{TDP43} (NDM vs ALS Staging)	R_{avg} (Average R)
Insula	0.41	0.45	−0.64	0.55
Putamen	0.51	0.42	−0.65	0.53
Pallidum	0.48	0.44	−0.61	0.53
Caudate	0.32	0.40	−0.52	0.46
Precentral	0.59	0.39	−0.42	0.40
Thalamus	0.50	0.47	−0.30	0.38

R_{max}- Maximum Pearson Correlation

Table 2

Correlation between individual subjects R_{max} and clinical scores

Correlation between R_{max} from individual subjects from insula seeding and UMN	R = 0.2363, p = 0.0488
Correlation between R_{max} from individual subjects from insula seeding and ALSFRS	R = 0.1518, p = 0.2097
Correlation between R_{max} from individual subjects from best seeds for each subject and UMN	R = 0.1337, p = 0.2698
Correlation between R_{max} from individual subjects from best seeds for each subject and ALSFRS	R = −0.0583, p = 0.6315

Table 3

Postmortem histopathological stages for each of 43 bilateral regions.

Region Names	Stages	Schmidt et al mapping	Region Names	Stages	Schmidt et al mapping
Bankssts	5	-	Precentral	1	1
Caudalanteriorcingulate	3	-	Precuneus	5	-
Caudalmiddlefrontal	2	2	Rostralanteriorcingulate	3	-
Cuneus	5	-	Rostralmiddlefrontal	3	2
Entorhinal	4	4	Superiorfrontal	2	1
Fusiform	5	-	Superiorparietal	4	-
Inferiorparietal	5	-	Superiortemporal	4	-
Inferiortemporal	5	-	Supramarginal	4	-
Isthmuscingulate	5	-	Frontalpole	3	-
Lateraloccipital	5	-	Temporalpole	4	-
Lateralorbitofrontal	3	3	Transversetemporal	4	-
Lingual	5	-	Insula	3	-
Medialorbitofrontal	3	3	CerebellumCortex	5	-
Middletemporal	4	-	ThalamusProper	3	-
Parahippocampal	4	-	Caudate	3	3
Paracentral	3	-	Putamen	3	3
Parsopercularis	3	-	Pallidum	3	-
Parsorbitalis	3	-	Hippocampus	4	4
Parstriangularis	3	-	Amygdala	4	-
Pericalcarine	5	-	Accumbensarea	3	3
Postcentral	3	3	Hypothalamus	4	-
Posteriorcingulate	5	-			